Journal of Applied Physics

RESEARCH ARTICLE | FEBRUARY 28 2024

AlGaN/GaN devices with metal–semiconductor or insulator–semiconductor interfacial layers: Vacuum level step due to dipole and interface fixed charge

Yuchen Deng ; Jieensi Gelan ; Kazuya Uryu ; Toshi-kazu Suzuki

J. Appl. Phys. 135, 084504 (2024)
https://doi.org/10.1063/5.0186457

Journal of Applied Physics ARTICLE pubs.aip.org/aip/jap

AlGaN/GaN devices with metal–semiconductor or insulator–semiconductor interfacial layers: Vacuum level step due to dipole and interface fixed charge

Cite as: J. Appl. Phys. **135**, 084504 (2024); doi: 10.1063/5.0186457
Submitted: 6 November 2023 · Accepted: 6 February 2024 ·
Published Online: 28 February 2024

Yuchen Deng,[1] Jieensi Gelan,[1] Kazuya Uryu,[2] and Toshi-kazu Suzuki[1,a)]

AFFILIATIONS

[1]Center for Nano Materials and Technology, Japan Advanced Institute of Science and Technology (JAIST), 1-1 Asahidai, Nomi, Ishikawa 923-1292, Japan
[2]Advantest Laboratories Ltd., 48-2 Matsubara, Kami-Ayashi, Aoba-ku, Sendai, Miyagi 989-3124, Japan

[a)]**Author to whom correspondence should be addressed:** tosikazu@jaist.ac.jp

ABSTRACT

We have systematically investigated effects of metal–semiconductor or insulator–semiconductor interfacial layers (ILs) in AlGaN/GaN devices, where AlO_x, TiO_x, or NiO_x is employed as an IL. From capacitance–voltage characteristics of metal/IL/AlGaN/GaN devices with a metal–semiconductor IL between the gate metal and AlGaN, it is shown that the IL modulates the threshold voltage V_{th}, attributed to the vacuum level step induced by the dipole of the IL. We find negative vacuum level steps for AlO_x and TiO_x ILs, and positive for NiO_x, from which the IL dipole density is estimated for each IL material. The two-dimensional electron gas carrier concentration in the metal/IL/AlGaN/GaN devices is also modulated by the vacuum level step. On the other hand, from capacitance–voltage characteristics of metal/Al_2O_3/IL/AlGaN/GaN devices with an insulator–semiconductor IL between Al_2O_3 and AlGaN, the fixed charge density of the Al_2O_3/IL/AlGaN interface is evaluated by the Al_2O_3 thickness dependence of V_{th}. For AlO_x and TiO_x ILs, the fixed charge density is higher than that of the Al_2O_3/AlGaN interface with no IL, while lower for NiO_x. The fixed charge density for an IL shows a positive correlation with the IL dipole density, suggesting that the fixed charge is related to the unbalanced IL dipole. Furthermore, using the conductance method, we find a low trap density of the Al_2O_3/IL/AlGaN interface for AlO_x and NiO_x ILs, in comparison with that of the Al_2O_3/AlGaN interface with no IL.

I. INTRODUCTION

Utilizing high-density two-dimensional electron gases (2DEGs), AlGaN/GaN Schottky and metal–insulator–semiconductor (MIS) field-effect transistors (FETs) have been extensively investigated, where the metal–semiconductor and insulator–semiconductor interfaces are important building blocks, affecting the threshold voltage V_{th} of the devices. In the case of the Schottky devices, V_{th} is dominated by the metal–semiconductor barrier height ϕ_S, which can be modulated by using metals with different work functions.[1,2] However, in many cases of GaN-based Schottky contacts, the value of ϕ_S is not uniquely determined by the difference between the metal work function and the (Al)GaN electron affinity, and is affected by treatments of the metal–semiconductor interface.[3–5] This indicates the existence of an unintentional metal–semiconductor interfacial layer, leading to a modulation of ϕ_S by a vacuum level step ΔE_{vac} due to a dipole of the interfacial layer.[6] On the other hand, in the case of the MIS devices, V_{th} is affected by the insulator–semiconductor conduction band offset φ and the fixed charge density σ_{int} of the insulator–semiconductor interface. Various insulators such as oxides Al_2O_3,[7] HfO_2,[8,9] TiO_2,[10] AlSiO,[11,12] AlTiO,[13–19] oxynitrides TaON,[20] AlON,[21] and nitrides BN,[22,23] AlN[24–28] have been employed as a gate insulator for GaN-based devices, where V_{th} can be modulated by both φ and σ_{int}. Similarly to ϕ_S, φ is not uniquely determined by the electron affinity difference between the insulator and the semiconductor, and is affected by insulator–semiconductor interface treatments.[29] Meanwhile, when an insulator such as Al_2O_3 is deposited on the Ga-polar (Al)GaN surface with a negative surface polarization charge, the fixed charge tends to be positive, neutralizing the

polarization charge,[30–37] while this is not always the case.[18,38,39] The behavior of φ and σ_{int} also can be attributed to the existence of an unintentional insulator–semiconductor interfacial layer with a dipole, where the band offset is modulated by ΔE_{vac} due to the dipole, and σ_{int} can be interpreted as a dipole unbalance. In order to control V_{th} of the AlGaN/GaN devices, an insertion of an intentional metal–AlGaN or insulator–AlGaN interfacial layer should be effective. A thin interfacial layer causes a vacuum level step ΔE_{vac} due to the interfacial layer dipole and a fixed charge density σ_{int} due to the dipole unbalance, modulating V_{th} similarly to the unintentional ones. Previously, intentional metal-(Al)GaN interfacial layers have been studied,[40,41] and MIS device performance improvements by intentional insulator–(Al)GaN interfacial layers have been reported.[42–44] However, systematic investigations have been lacking on intentional metal-(Al)GaN and insulator–(Al)GaN interfacial layers.

In this work, effects of metal–semiconductor or insulator–semiconductor interfacial layers (ILs) in AlGaN/GaN devices were systematically investigated, where thin AlO_x, TiO_x, or NiO_x obtained by metal layer oxidation is employed as an IL. We fabricated metal/IL/AlGaN/GaN devices and obtained their capacitance–voltage (C–V) characteristics, from which we find modulation of the threshold voltage V_{th} due to the vacuum level step ΔE_{vac} induced by the dipole of the metal–AlGaN IL. From the vacuum level steps, the IL dipole density is estimated for each IL material. Using Hall measurements for the metal/IL/AlGaN/GaN devices, it is shown that the 2DEG carrier concentration is also modulated by ΔE_{vac}. We also fabricated metal/Al_2O_3/IL/AlGaN/GaN devices and obtained their C-V characteristics. From the Al_2O_3 thickness dependence of V_{th}, we find the fixed charge density of the Al_2O_3/IL/AlGaN interface, showing a positive correlation with the IL dipole density. Furthermore, we characterized the interface trap density in the metal/Al_2O_3/IL/AlGaN/GaN devices using the conductance method.

II. EFFECTS OF METAL–SEMICONDUCTOR INTERFACIAL LAYERS (ILs) IN METAL/IL/AlGaN/GaN DEVICES

Using an $Al_{0.24}Ga_{0.76}N$ (20 nm)/GaN (3 μm) heterostructure grown by metal-organic vapor phase epitaxy on a sapphire (0001) substrate, we fabricated metal/IL/AlGaN/GaN capacitor devices with a gate area of $75^2\,\mu m^2$, whose schematic is shown in Fig. 1(a). After Ti-based Ohmic electrode formation, thin Al, Ti, or Ni metal layers with several thicknesses in the nm-range were deposited on AlGaN. Annealing at 350 °C in air was carried out next, to obtain thin oxide ILs of AlO_x, TiO_x, or NiO_x. Figure 2 shows examples of atomic force microscope (AFM) images for the surfaces of the AlO_x, TiO_x, and NiO_x ILs in comparison with the AlGaN surface, indicating that the surface morphology is unchanged after the IL formation. Although we found thickness increases by a few tens of percent for the ILs from the original metal layers by AFM, suggesting oxidation of the ILs, the observed thickness values lack accuracy. Thus, we employed estimation of the IL thicknesses d_{IL} by the IL capacitance $C_{IL} \propto 1/d_{IL}$ as shown later. On the other hand, oxidation was confirmed by separate experiments of measuring the sheet resistance of the metal layers before and after annealing on insulating sapphire substrates, where at least 10^5 times increased sheet resistances were observed after annealing, indicating that the annealing condition is enough to obtain the oxide ILs. The fabrication was completed by the formation of the Ni gate metal covered by Au. Metal/AlGaN/GaN capacitor devices with no IL were also fabricated for comparison.

Figure 3 shows examples of current–voltage (J–V) characteristics of the fabricated devices, where one device is picked up for each IL, under application of the gate voltage V_G with respect to the grounded Ohmic electrode. The IL leads to lower leakage, which can be attributed to both the vacuum level steps ΔE_{vac} (equivalently the effective barrier height ϕ_S) and the IL barrier effects. Thus, it is difficult to accurately evaluate ΔE_{vac} (or ϕ_S) from the J–V characteristics. On the other hand, ΔE_{vac} can be evaluated from the capacitance–voltage (C–V) characteristics. Figure 1(b) shows the band diagram of a metal/IL/AlGaN/GaN device, where ϕ_{S0} is the barrier height with no vacuum level step, ϕ_S is the effective barrier height, ΔE_c is the AlGaN–GaN conduction band offset, $\sigma_{GaN}/q \simeq 2.1 \times 10^{13}\,cm^{-2}$ and $\sigma_{AlGaN}/q \simeq 3.2 \times 10^{13}\,cm^{-2}$ give the polarization charge densities,[45–49] and σ_D is the IL dipole density. From this band diagram, we obtain the vacuum level step

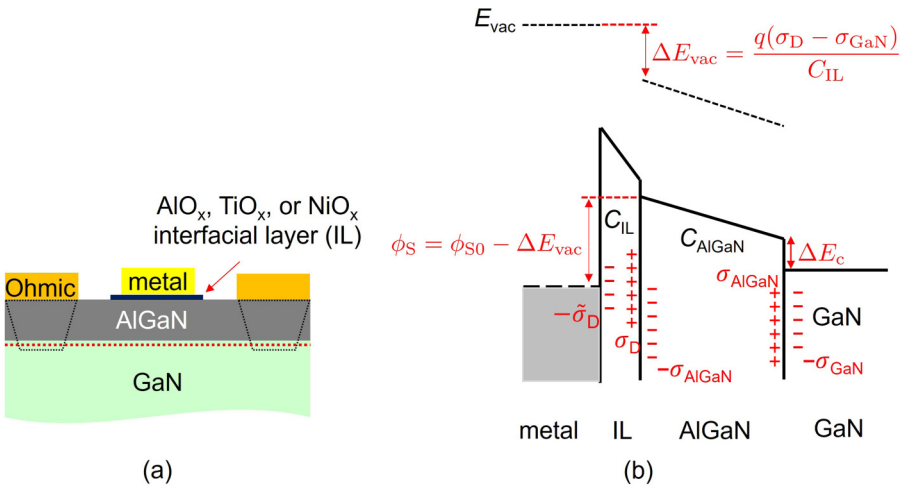

FIG. 1. (a) The schematic and (b) the band diagram of the metal/IL/AlGaN/GaN devices.

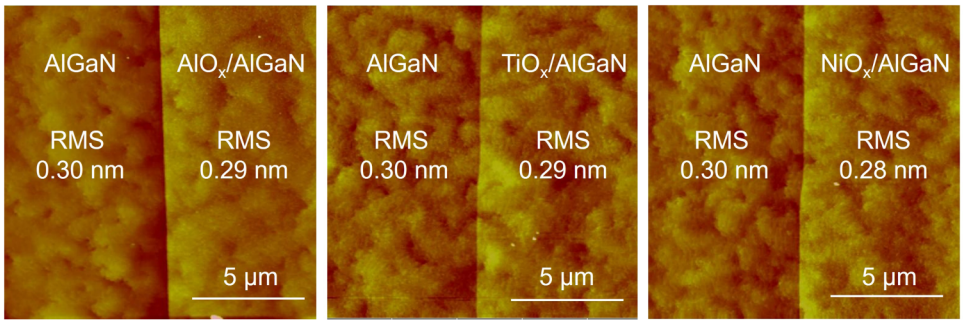

FIG. 2. Atomic force microscope (AFM) images of the surfaces of AlGaN, AlO_x, TiO_x, and NiO_x.

$$\Delta E_{\mathrm{vac}} = \frac{q(\sigma_{\mathrm{D}} - \sigma_{\mathrm{GaN}})}{C_{\mathrm{IL}}} = \frac{q(\sigma_{\mathrm{D}} - \sigma_{\mathrm{GaN}})}{k_{\mathrm{IL}}\epsilon_0} d_{\mathrm{IL}}, \tag{1}$$

and the threshold voltage

$$V_{\mathrm{th}} = \frac{\phi_{\mathrm{S0}}}{q} - \frac{\Delta E_{\mathrm{vac}}}{q} - \frac{\sigma_{\mathrm{AlGaN}} - \sigma_{\mathrm{GaN}}}{C_{\mathrm{AlGaN}}} - \frac{\Delta E_{\mathrm{C}}}{q}, \tag{2}$$

using the IL capacitance C_{IL}, the IL dielectric constant k_{IL}, the IL thickness d_{IL}, and the AlGaN capacitance C_{AlGaN}. Since the threshold voltage with no IL is given by

$$V_{\mathrm{th0}} = \frac{\phi_{\mathrm{S0}}}{q} - \frac{\sigma_{\mathrm{AlGaN}} - \sigma_{\mathrm{GaN}}}{C_{\mathrm{AlGaN}}} - \frac{\Delta E_{\mathrm{C}}}{q}, \tag{3}$$

assuming $\Delta E_{\mathrm{vac}} = 0$, we obtain the threshold voltage shift

$$V_{\mathrm{th}} - V_{\mathrm{th0}} = -\frac{\Delta E_{\mathrm{vac}}}{q}, \tag{4}$$

which can be used to evaluate ΔE_{vac}. Figure 4 shows examples of C–V characteristics at frequency $f = 1$ MHz, where one device is picked up for each IL. The 2DEG concentration n_{s} obtained by

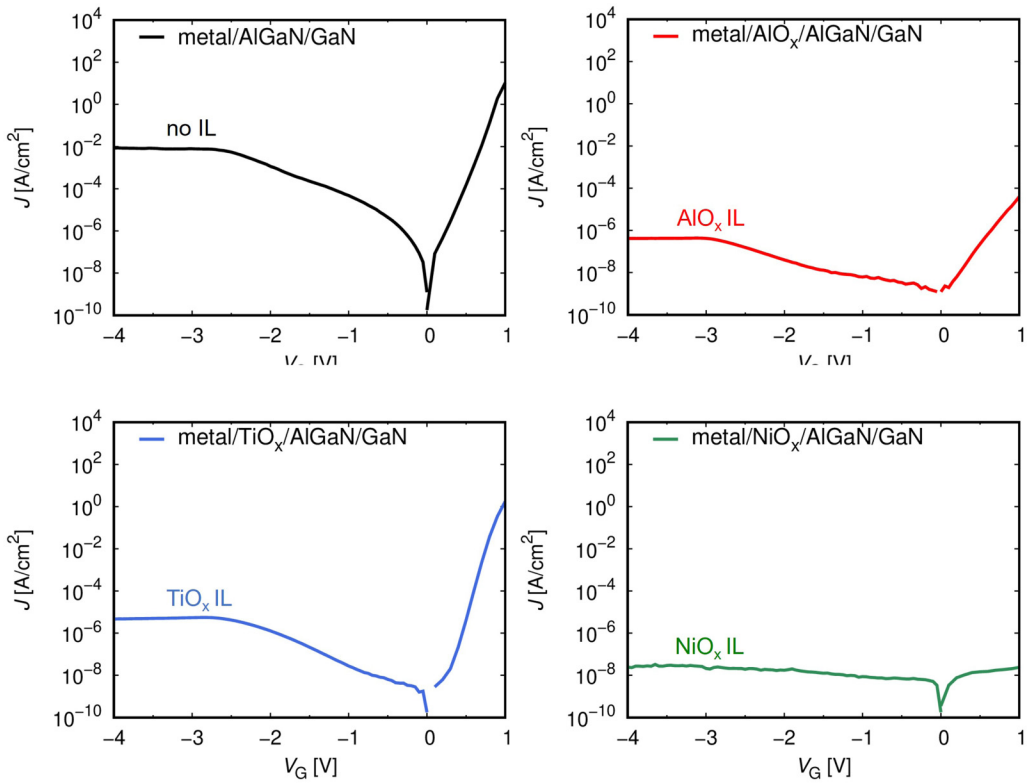

FIG. 3. *J*–*V* characteristics of metal/AlGaN/GaN and metal/IL/AlGaN/GaN devices.

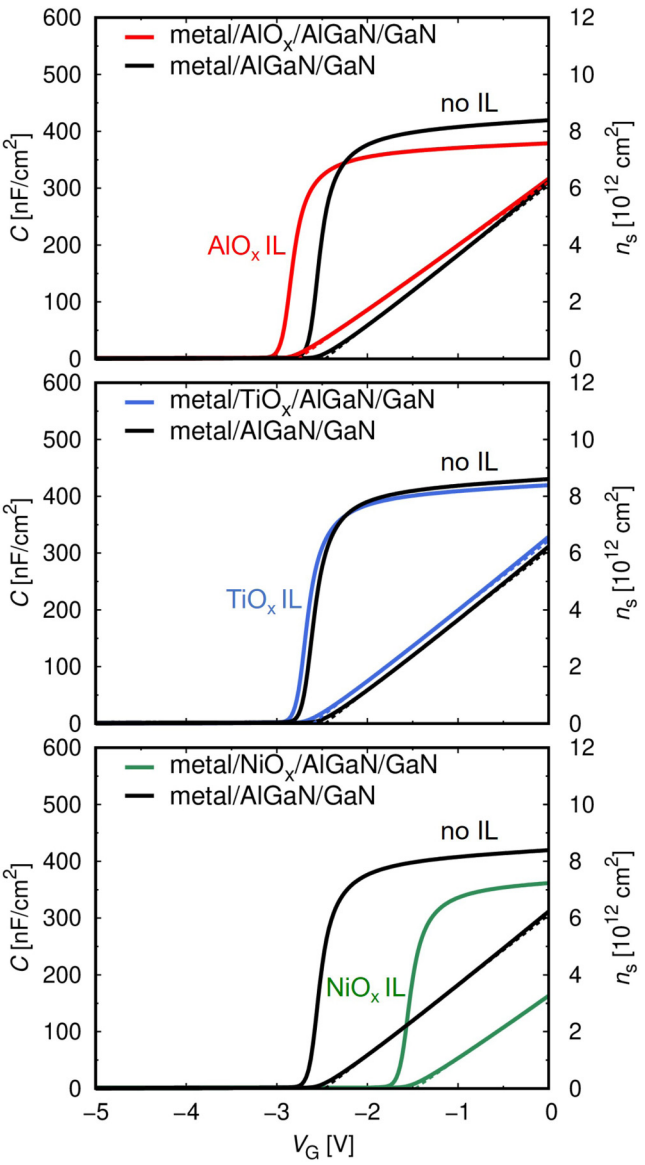

FIG. 4. *C–V* characteristics of metal/AlGaN/GaN and metal/IL/AlGaN/GaN devices.

integrating the *C–V* characteristics is also shown in Fig. 4 and can be fitted by $qn_s \simeq C_{tot}(V_G - V_{th})$ using the total capacitance C_{tot} given by $1/C_{tot} = 1/C_{AlGaN} + 1/C_{IL}$. From the fitting, V_{th}, V_{th0}, C_{AlGaN}, and C_{IL} are obtained for all the devices with several IL thicknesses d_{IL}. Since $1/C_{IL} = d_{IL}/k_{IL}\varepsilon_0$, we obtain d_{IL} by assuming typical dielectric constants ~7 of AlO_x, ~30 of TiO_x, and ~10 of NiO_x. The obtained $1/C_{IL}$ and d_{IL} are summarized in Table I. The obtained $V_{th} - V_{th0}$ and ΔE_{vac} of all the devices are shown in Fig. 5 as functions of $1/C_{IL}$, where $V_{th} - V_{th0}$ and $-\Delta E_{vac}$ are shown in the left and right vertical axes, respectively. It is shown

TABLE I. $1/C_{IL}$ and d_{IL}.

	AlO_x	TiO_x	NiO_x
$1/C_{IL}$ (cm^2/μF)	0.20–0.43	0.01–0.08	0.20–0.38
d_{IL} (nm)	1.4–2.8	0.3–2.4	2.0–3.8

that $V_{th} - V_{th0} < 0$ for the AlO_x and TiO_x ILs, indicating that the vacuum level step ΔE_{vac} is positive, while for the NiO_x ILs, $V_{th} - V_{th0} > 0$ indicating that the vacuum level step ΔE_{vac} is negative. Moreover, we find an almost proportional relation $\Delta E_{vac} \propto 1/C_{IL} \propto d_{IL}$ for each IL, indicating that the IL dipole density

$$\sigma_D = \frac{\Delta E_{vac} C_{IL}}{q} + \sigma_{GaN} \tag{5}$$

is almost constant for each IL material. Figure 6 shows the averaged IL dipole densities in comparison with σ_{AlGaN}, $\sigma_D/q \simeq 2.5 \times 10^{13}$ cm^{-2} of the AlO_x ILs, $\sigma_D/q \simeq 3.5 \times 10^{13}$ cm^{-2} of the TiO_x ILs, and $\sigma_D/q \simeq 0.4 \times 10^{13}$ cm^{-2} of the NiO_x ILs, where the error bars stand for the three-sigma standard deviations. This indicates that the AlO_x/AlGaN and TiO_x/AlGaN interfaces are nearly neutral, while the NiO_x/AlGaN interface is quite negatively charged.

Moreover, we fabricated metal/IL/AlGaN/GaN and metal/AlGaN/GaN Hall-bar devices shown in the inset of Fig. 7. From Hall measurements under a magnetic field $B = 0.32$ T, the 2DEG carrier concentration n_{s0} at $V_G = 0$ was obtained. The relation between qn_{s0}/C_{tot} and ΔE_{vac} is shown in Fig. 7, being consistent with $qn_{s0}/C_{tot} = -V_{th} = \Delta E_{vac}/q + V_{th0}$ shown by the dashed line, indicating that the 2DEG carrier concentration n_{s0} is also modulated by the vacuum level step ΔE_{vac} due to the dipole. In particular, the NiO_x ILs strongly reduce the 2DEG concentration.

The fact that ΔE_{vac} is either positive or negative can be attributed to the reaction at the IL/AlGaN interface. The tie-line configurations for metal-(Al)Ga-N systems have been studied,[50,51] showing that TiN is stable in a Ti–(Al)Ga–N system, while NiGa is stable in a Ni–(Al)Ga–N system. Considering that AlN is also stable in a

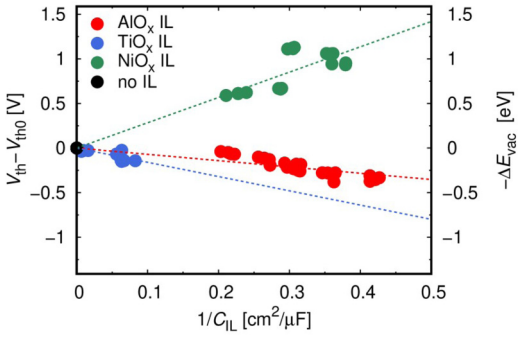

FIG. 5. The threshold voltage shift $V_{th} - V_{th0}$ and vacuum level step ΔE_{vac} of all the devices as functions of $1/C_{IL}$.

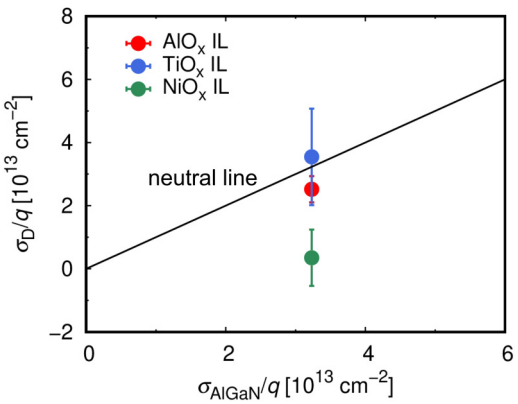

FIG. 6. The interfacial layer (IL) dipole density σ_D in comparison with the AlGaN polarization charge density σ_{AlGaN}.

Al–(Al)Ga–N system, due to the formation of TiN or AlN, nitrogen vacancy V_N donors can be generated at the TiO_x/AlGaN or AlO_x/AlGaN interface, and the ionized donors act as positive IL dipole charges leading to the positive ΔE_{vac}. On the other hand, due to the formation of NiGa, gallium vacancy V_{Ga} acceptors can be generated at the NiO_x/AlGaN interface, and the ionized acceptors can negatively contribute to the IL dipole charges leading to the negative ΔE_{vac}.

III. EFFECTS OF INSULATOR–SEMICONDUCTOR ILs IN METAL/Al_2O_3/IL/AlGaN/GaN DEVICES

Using the same AlGaN/GaN heterostructure, for the AlO_x, TiO_x, or NiO_x ILs, we fabricated metal/Al_2O_3/IL/AlGaN/GaN capacitor devices with a gate area of $75^2\,\mu m^2$, whose schematic is shown in Fig. 8(a). After the IL formation, several thicknesses of

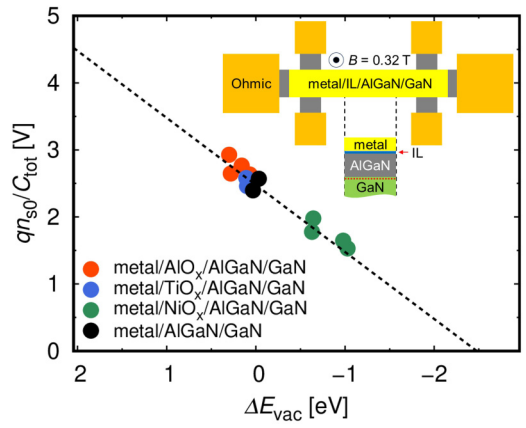

FIG. 7. The relation between n_{s0} obtained by Hall measurements and ΔE_{vac}. The dashed line shows $qn_{s0}/C_{tot} = -V_{th} = \Delta E_{vac}/q + V_{th0}$. Inset: the schematic of the Hall-bar devices.

Al_2O_3 gate insulators were formed by atomic layer deposition (ALD) using TMA (trimethyl aluminum) and water. The fabrication was completed by the formation of the Ni gate metal covered by Au. Metal/Al_2O_3/AlGaN/GaN capacitor devices with no IL were also fabricated for comparison.

Figure 8(b) shows the band diagram of a metal/Al_2O_3/IL/AlGaN/GaN device, from which the threshold voltage V_{th} is given by

$$V_{th} = \frac{\phi}{q} - \frac{\sigma_{int} - \sigma_{GaN}}{C_{Al_2O_3}} - \frac{\varphi}{q} - \frac{\sigma_{AlGaN} - \sigma_{GaN}}{C_{AlGaN}} - \frac{\Delta E_C}{q}$$
$$= \frac{\sigma_{GaN} - \sigma_{int}}{k_{Al_2O_3}\epsilon_0} d_{Al_2O_3} - \frac{\sigma_{AlGaN} - \sigma_{GaN}}{C_{AlGaN}} + \frac{\phi - \varphi - \Delta E_C}{q}, \quad (6)$$

where $C_{Al_2O_3} = k_{Al_2O_3}\varepsilon_0/d_{Al_2O_3}$ is the Al_2O_3 capacitance given by the Al_2O_3 dielectric constant $k_{Al_2O_3}$ and the thickness $d_{Al_2O_3}$, ϕ is the metal–Al_2O_3 barrier height, φ is the effective Al_2O_3–AlGaN conduction band offset, $\sigma_{int} = \sigma_D - \tilde{\sigma}_D$ is the fixed charge density of the Al_2O_3/IL/AlGaN interface due to the unbalanced IL dipole. It should be noted that V_{th} is a linear function of $d_{Al_2O_3}$, where the slope is $(\sigma_{GaN} - \sigma_{int})/(k_{Al_2O_3}\varepsilon_0)$, and the intercept is $-(\sigma_{AlGaN} - \sigma_{GaN})/C_{AlGaN} + (\phi - \varphi - \Delta E_C)/q$. From the former, we can evaluate σ_{int} due to the unbalanced IL dipole. Also the latter is determined by $\phi - \varphi$, where φ is affected by the vacuum level step ΔE_{vac} induced by the dipole of the insulator–AlGaN IL.

Figure 9 shows examples of C–V characteristics at $f = 1$ MHz. The 2DEG concentration n_s obtained by integrating the C–V characteristics is also shown in Fig. 9, and fitted by $qn_s \simeq C_{tot}(V_G - V_{th})$ using the total capacitance C_{tot} given by $1/C_{tot} = 1/C_{Al_2O_3} + 1/C_{AlGaN} + 1/C_{IL} = d_{Al_2O_3}/(k_{Al_2O_3}\varepsilon_0) + 1/C_{AlGaN} + 1/C_{IL}$. From the fitting, we obtain C_{tot} and V_{th}. Examples of $1/C_{tot}$ are shown in Fig. 10(a) as functions of the Al_2O_3 insulator thickness $d_{Al_2O_3}$. By linear fitting of $1/C_{tot}$-$d_{Al_2O_3}$, we obtain $k_{Al_2O_3}$ from the slope, and C_{AlGaN} and C_{IL} from the intercepts at $d_{Al_2O_3} = 0$. Figure 10(b) shows examples of V_{th} as functions of $d_{Al_2O_3}$, where the AlO_x and TiO_x ILs lead to more negative V_{th} shifts, while the NiO_x ILs lead to less negative ones. By linear fitting using Eq. (6), we evaluate σ_{int} shown in Fig. 11 as functions of $1/C_{IL}$ with error bars standing for the three-sigma asymptotic standard errors of the linear fittings. Although the error bars are slightly large, σ_{int} is almost independent of $1/C_{IL}$ for each IL, and the averaged σ_{int}/q are $\simeq 3.2 \times 10^{13}$ cm^{-2} for no IL (the error bar is indicated by two dashed lines), $\simeq 3.6 \times 10^{13}$ cm^{-2} for the AlO_x ILs, $\simeq 3.9 \times 10^{13}$ cm^{-2} for the TiO_x ILs, and $\simeq 2.7 \times 10^{13}$ cm^{-2} for the NiO_x ILs. Using the IL dipole density σ_D obtained for each IL material in the previous section, the relation between σ_{int} and σ_D is demonstrated in Fig. 12, showing a positive correlation. This suggests that the fixed charge is related to the unbalanced IL dipole. On the other hand, assuming a metal–Al_2O_3 barrier height $\phi = 4.6$ eV,[18] the effective Al_2O_3–AlGaN conduction band offsets are evaluated to be $\varphi \simeq 2.1 \pm 1$ eV for no IL, $\varphi \simeq 2.5$ eV for the NiO_x ILs, and $\varphi \sim 0$–5 eV for the AlO_x or TiO_x ILs, where the uncertainty comes from the asymptotic standard errors of the linear fitting. Owing to this large uncertainty, unfortunately it is difficult to discuss φ affected by the vacuum level step ΔE_{vac}.

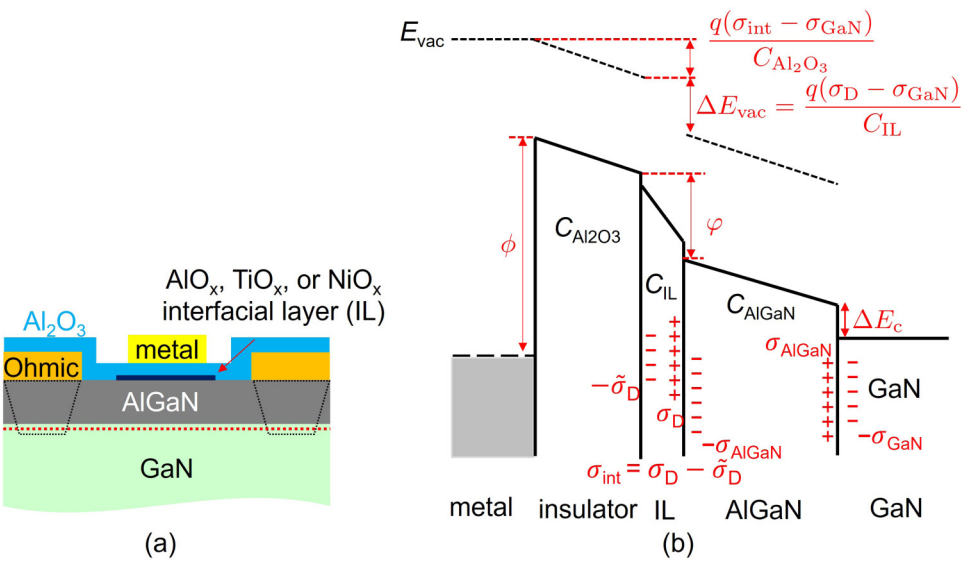

FIG. 8. (a) The schematic and (b) the band diagram of the metal/Al_2O_3/IL/AlGaN/GaN devices.

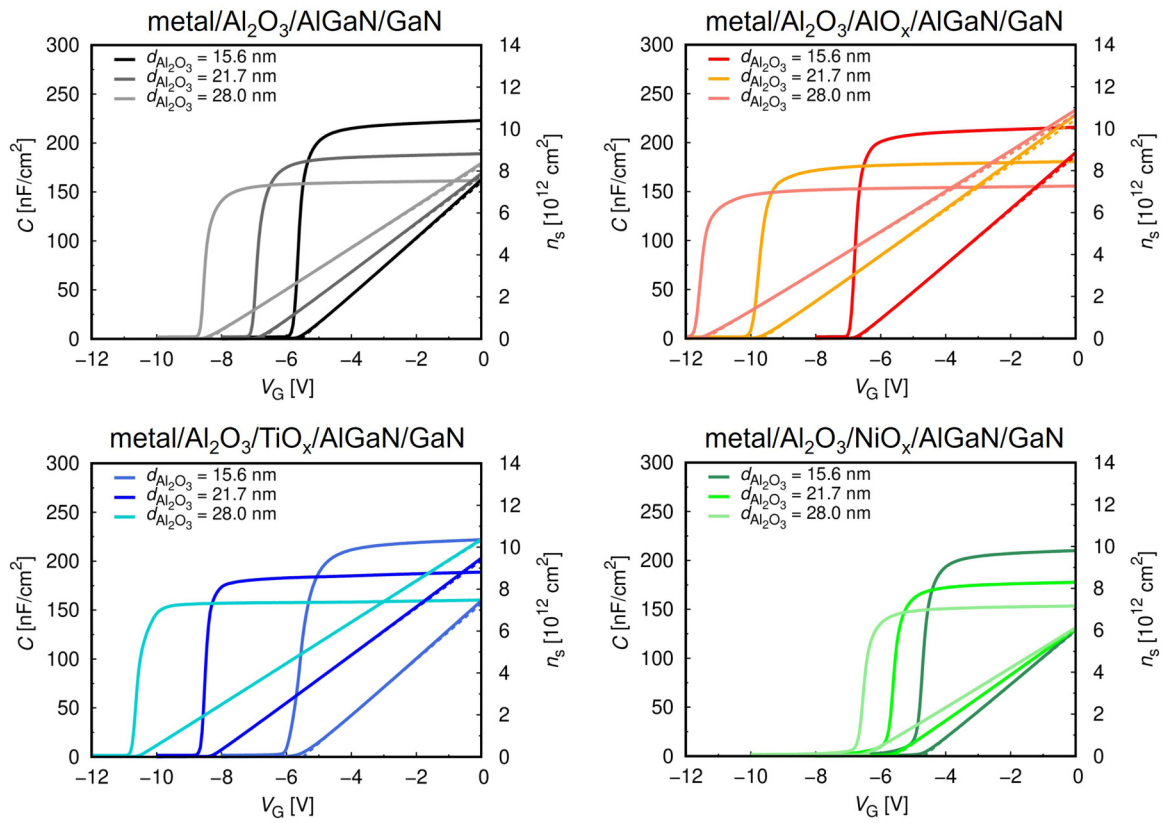

FIG. 9. *C–V* characteristics of metal/Al_2O_3/AlGaN/GaN and metal/Al_2O_3/IL/AlGaN/GaN devices.

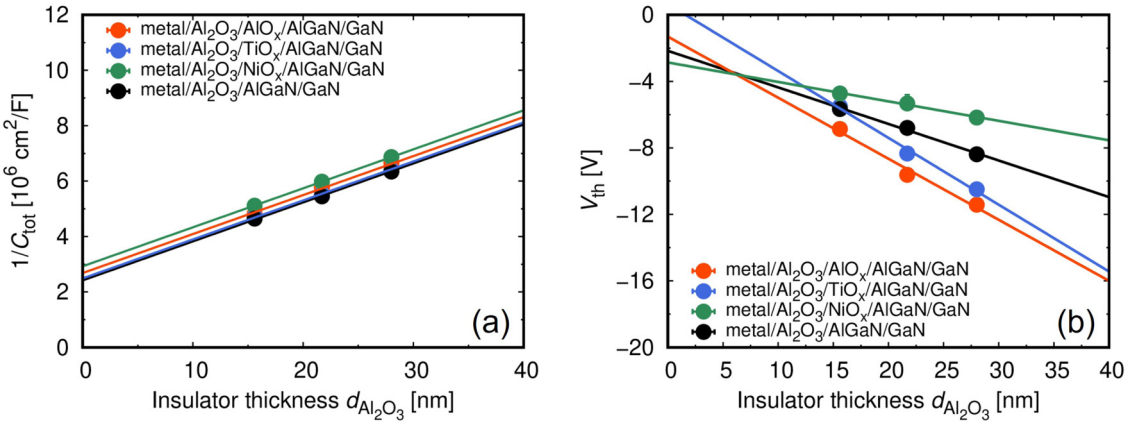

FIG. 10. (a) The inverse of total capacitances $1/C_{tot}$ and (b) threshold voltages V_{th} depending on the insulator thicknesses $d_{Al_2O_3}$.

There is a concern that the IL may increase the interface trap density. Thus, we characterized the trap densities of the Al_2O_3/IL/AlGaN interfaces by f-dependent C–V measurements for $f = 100$–1 MHz. While negligible hystereses were observed for reverse bias applications, hystereses take place for high forward bias applications, being independent of the ILs and thus attributed to deep traps inside the Al_2O_3. In order to avoid influences of the hystereses on the frequency dispersion characterization, we employed frequency sweeps (instead of bias sweeps) at each fixed bias for the measurements. Therefore, the frequency dispersion characterization is not influenced by the hysteresis effect. Examples of f-dependent C-V characteristics of devices with $d_{Al_2O_3} = 22$ nm are shown in Fig. 13, where the measured data were plotted at each fixed frequency. Negligible frequency dispersion is observed in the negative bias region for all the devices, showing that the V_{th} determination is not affected by the measurement frequency. On the other hand, frequency dispersions are observed for positive biases except for the TiO_x ILs. By using the conductance method,[52] which is widely employed for interface characterization,[15,35,53] the interface trap density was evaluated using the equivalent circuits shown in the inset of Fig. 13. Figure 14 shows examples of G_{it}/ω ($\omega = 2\pi f$) as functions of frequency f, exhibiting single-peaked behaviors except for the TiO_x ILs. These single-peaked behaviors are described by

$$\frac{G_{it}}{\omega} = \frac{q^2 D_{it} \ln(1+\omega^2\tau^2)}{2\omega\tau}, \tag{7}$$

where the electron trapping time constant τ is given by the peak frequency $f_p = 1/(\pi\tau)$, and the interface trap density D_{it} by the peak value $G_{it}/\omega \simeq 0.4q^2 D_{it}$. The absence of single-peaked behavior for the TiO_x ILs suggests that the interface traps have a very

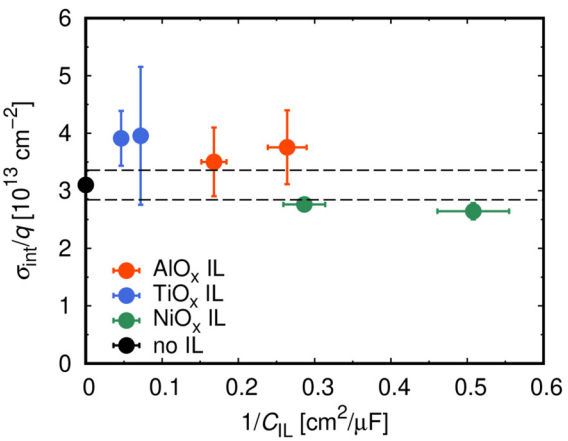

FIG. 11. The relation between the fixed charge density σ_{int} and $1/C_{IL}$.

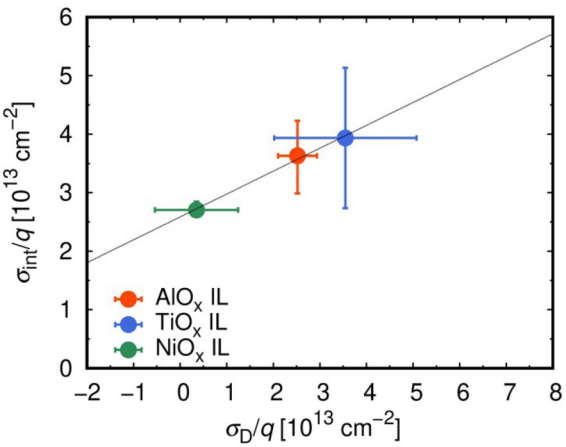

FIG. 12. The relation between the fixed charge density σ_{int} and the IL dipole density σ_D.

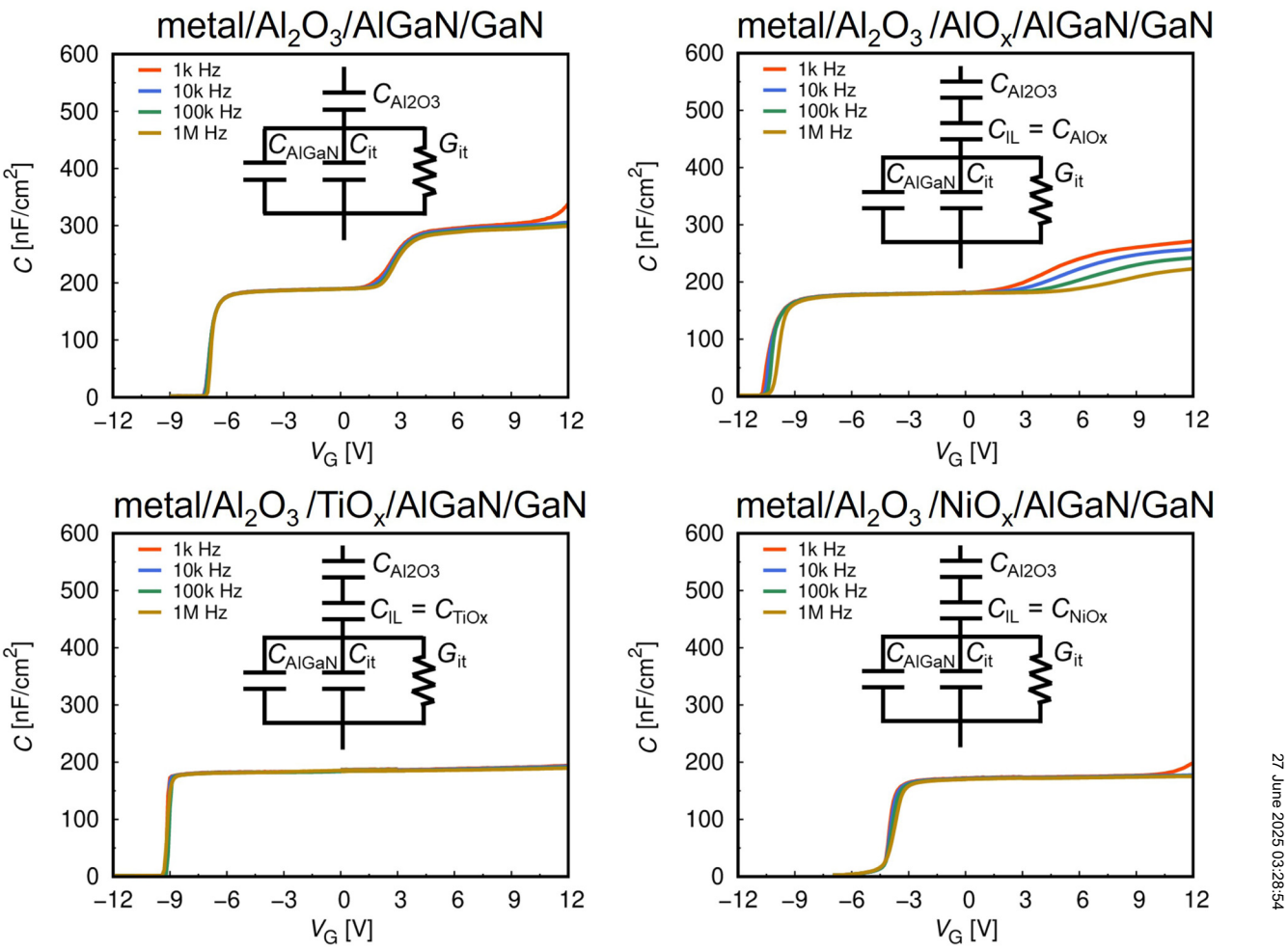

FIG. 13. f-dependent C–V characteristics of metal/Al_2O_3/AlGaN/GaN and metal/Al_2O_3/ IL/AlGaN/GaN devices. Insets: the equivalent circuits.

long trapping time constant. The peak values of G_{it}/ω are shown in the inset of Fig. 15 as functions of frequency. For an interface trap at the energy E, the time constant τ at temperature T is given by

$$\tau = e^{(E_C-E)/k_BT}/(\nu_{th}\sigma_e N_C) = \tau_0\, e^{(E_C-E)/k_BT}, \quad (8)$$

using the conduction band bottom energy E_C, the electron thermal velocity ν_{th}, the capture cross section of the trap σ_e, and the conduction band effective density of states N_C, where $\tau_0 = 1/(\nu_{th}\sigma_e N_C)$. Even though τ_0 is ambiguous due to the uncertain σ_e, by assuming a wide range of $\tau_0 \sim 0.1$–10^3 ps, D_{it} as functions of $E_C - E$ are evaluated and shown in Fig. 15, where the error bars correspond to the widely assumed τ_0. The interface trap densities are $D_{it} \simeq 2.5 \times 10^{13}\,cm^{-2}\,eV^{-1}$ for no IL, $D_{it} \simeq 1.6 \times 10^{13}\,cm^{-2}\,eV^{-1}$ for the AlO_x ILs, and $D_{it} \simeq 0.8 \times 10^{13}\,cm^{-2}\,eV^{-1}$ for the NiO_x ILs. This means that D_{it} for no IL is higher than those for the AlO_x and NiO_x ILs, despite of the apparently weak frequency dispersion in the C–V characteristics for no IL shown in Fig. 13. We consider that this behavior can be explained as follows. In Fig. 14 for no IL, in addition to the observed peak, we find the tail of another next peak of G_{it}/ω at $\lesssim 1$ MHz for forward biases, whose peak frequency is higher than the measurement frequency range and whose peak value is comparable to the observed peak. This indicates another kind of traps, which contribute to C_{it} in the form of $q^2 D_{it}\mathrm{atan}(\omega\tau)/\omega\tau$, and thus C_{it} becomes large ($\sim 10\,\mu F/cm^2$) in the measurement frequency range. Accordingly, we obtain the measured capacitance $C_m \simeq C_{Al_2O_3}$, which hardly shows frequency dispersion. On the other hand, we do not observe the second step of the C–V characteristics for the NiO_x IL shown in Fig. 13, indicating that electron trapping at the interface traps does not take place. This is owing to weak effects of G_{it} and D_{it} in the measurement frequency range, because of the peak frequency of G_{it}/ω in the 100 Hz range and the small peak value due to the

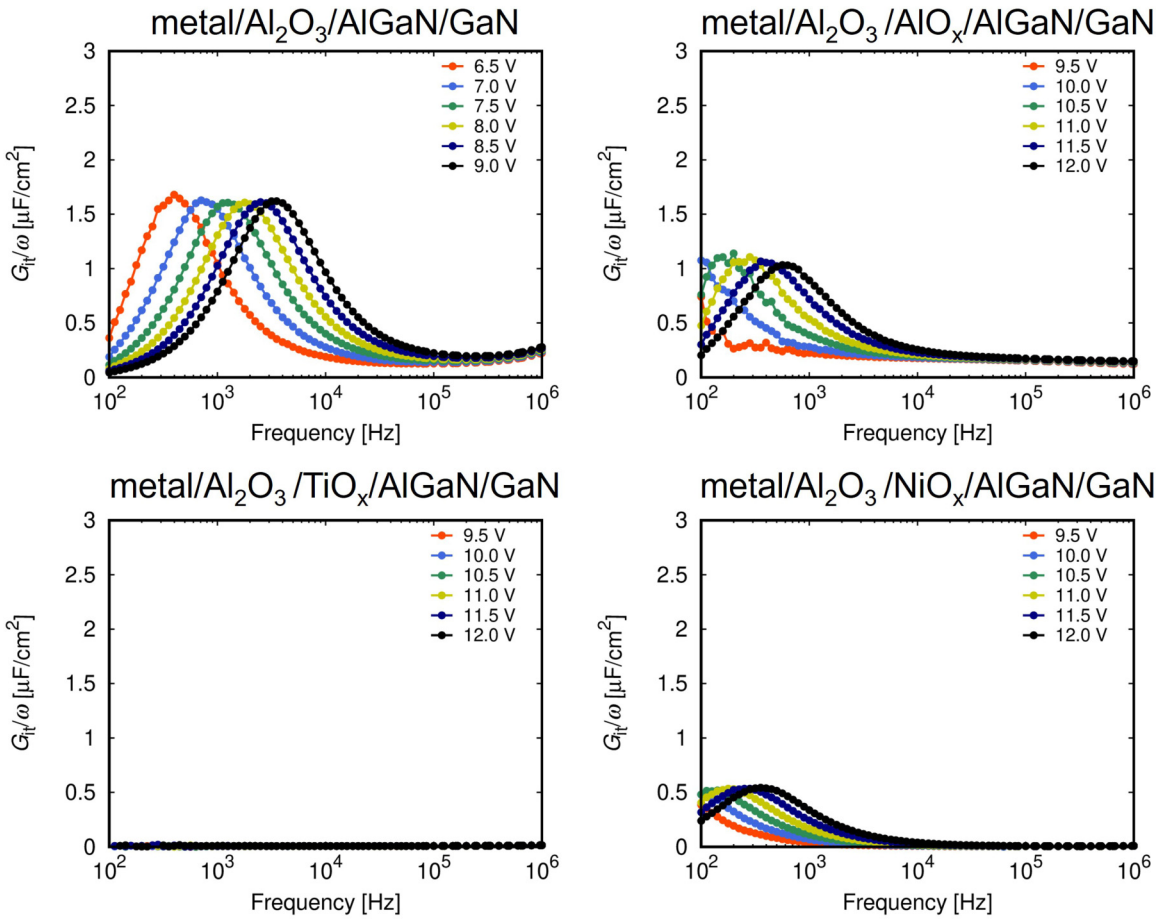

FIG. 14. G_{it}/ω as functions of frequency with fitting curves for metal/Al_2O_3/AlGaN/GaN and metal/Al_2O_3/ IL/AlGaN/GaN devices.

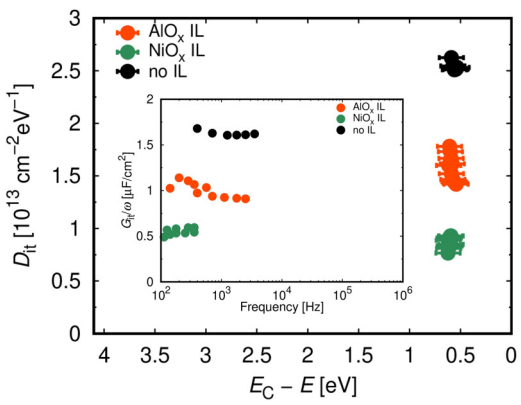

FIG. 15. The interface trap density D_{it} as functions of the energy $E_C - E$. Inset: the peak value of G_{it}/ω as functions of peak frequency.

low D_{it}. Thus, it is possible to conclude that the AlO_x and NiO_x ILs suppress the interface trap density.

IV. CONCLUSION

We systematically investigated effects of metal–semiconductor or insulator–semiconductor interfacial layers (ILs) in AlGaN/GaN devices, where AlO_x, TiO_x, or NiO_x is employed as an IL. From capacitance–voltage characteristics of metal/IL/AlGaN/GaN devices, it is shown that the metal–AlGaN IL leads to modulation of the threshold voltage V_{th}, attributed to the vacuum level step induced by the IL dipole. We find negative vacuum level steps for AlO_x and TiO_x, and positive for NiO_x, from which the IL dipole density is estimated, indicating that the AlO_x/AlGaN and TiO_x/AlGaN interfaces are nearly neutral, while the NiO_x/AlGaN interface is negatively charged. From Hall measurements, we find that the 2DEG carrier concentration in the metal/IL/AlGaN/GaN devices is also modulated by the vacuum level step. On the other

hand, from capacitance–voltage characteristics of metal/Al_2O_3/IL/AlGaN/GaN devices, the fixed charge density of the Al_2O_3/IL/AlGaN interface is evaluated. For AlO_x and TiO_x, the fixed charge density is increased in comparison with no IL, while decreased for NiO_x. The fixed charge density shows a positive correlation with the IL dipole density, suggesting that the fixed charge is related to the unbalanced IL dipole. Furthermore, using the conductance method, we show that it is possible to obtain small trap densities of metal/Al_2O_3/IL/AlGaN interfaces, comparing to the interface with no IL.

ACKNOWLEDGMENTS

This work was supported by Japan Society for the Promotion of Science (JSPS) Grants-in-Aid for Scientific Research (KAKENHI) Grant No. JP22H01545.

AUTHOR DECLARATIONS

Conflict of Interest

The authors have no conflicts to disclose.

Author Contributions

Yuchen Deng: Data curation (lead); Formal analysis (lead); Investigation (lead); Resources (lead); Writing – original draft (lead). **Jieensi Gelan:** Investigation (supporting). **Kazuya Uryu:** Resources (supporting); Writing – review & editing (supporting). **Toshi-kazu Suzuki:** Conceptualization (lead); Funding acquisition (lead); Methodology (lead); Project administration (lead); Supervision (lead); Writing – review & editing (lead).

DATA AVAILABILITY

The data that support the findings of this study are available from the corresponding author upon reasonable request.

REFERENCES

[1]Z. Lin, W. Lu, J. Lee, D. Liu, J. S. Flynn, and G. R. Brandes, Appl. Phys. Lett. **82**, 4364 (2003).
[2]G. Li, T. Zimmermann, Y. Cao, C. Lian, X. Xing, R. Wang, P. Fay, H. G. Xing, and D. Jena, IEEE Electron Device Lett. **31**, 954 (2010).
[3]C. T. Lee, Y.-J. Lin, and D.-S. Liu, Appl. Phys. Lett. **79**, 2573 (2001).
[4]K. A. Rickert, A. B. Ellis, F. J. Himpsel, J. Sun, and T. F. Kuech, Appl. Phys. Lett. **80**, 204 (2002).
[5]K. Isobe and M. Akazawa, AIP Adv. **8**, 115011 (2018).
[6]C. Wang and X. Li, Appl. Surf. Sci. **622**, 156954 (2023).
[7]T. Hashizume, S. Ootomo, and H. Hasegawa, Appl. Phys. Lett. **83**, 2952 (2003).
[8]C. Liu, E. F. Chor, and L. S. Tan, Appl. Phys. Lett. **88**, 173504 (2006).
[9]A. Kawano, S. Kishimoto, Y. Ohno, K. Maezawa, T. Mizutani, H. Ueno, T. Ueda, and T. Tanaka, Phys. Status Solidi C **4**, 2700 (2007).
[10]S. Yagi, M. Shimizu, M. Inada, Y. Yamamoto, G. Piao, H. Okumura, Y. Yano, N. Akutsu, and H. Ohashi, Solid State Electron. **50**, 1057 (2006).
[11]C. Gupta, S. H. Chan, A. Agarwal, N. Hatui, S. Keller, and U. K. Mishra, IEEE Electron Device Lett. **38**, 1575 (2017).
[12]D. Kikuta, K. Ito, T. Narita, and T. Kachi, Appl. Phys. Express **13**, 026504 (2020).
[13]S. P. Le, T. Ui, T. Q. Nguyen, H. A. Shih, and T. Suzuki, J. Appl. Phys. **119**, 204503 (2016).
[14]A. Colon, L. Stan, R. Divan, and J. Shi, J. Vac. Sci. Technol. A **35**, 01B132 (2017).
[15]S. P. Le, D. D. Nguyen, and T. Suzuki, J. Appl. Phys. **123**, 034504 (2018).
[16]S. Dutta Gupta, A. Soni, V. Joshi, J. Kumar, R. Sengupta, H. Khand, B. Shankar, N. Mohan, S. Raghavan, N. Bhat, and M. Shrivastava, IEEE Trans. Electron Devices **66**, 2544 (2019).
[17]D. D. Nguyen and T. Suzuki, J. Appl. Phys. **127**, 094501 (2020).
[18]D. D. Nguyen, T. Isoda, Y. Deng, and T. Suzuki, J. Appl. Phys. **130**, 014503 (2021).
[19]D. D. Nguyen, Y. Deng, and T. Suzuki, Semicond. Sci. Technol. **38**, 095010 (2023).
[20]T. Sato, J. Okayasu, M. Takikawa, and T. Suzuki, IEEE Electron Device Lett. **34**, 375 (2013).
[21]M. Nozaki, K. Watanabe, T. Yamada, H.-A. Shih, S. Nakazawa, Y. Anda, T. Ueda, A. Yoshigoe, T. Hosoi, T. Shimura, and H. Watanabe, Jpn. J. Appl. Phys. **57**, 06KA02 (2018).
[22]J.-C. Gerbedoen, A. Soltani, M. Mattalah, M. Moreau, P. Thevenin, and J.-C. D. Jaeger, Diamond Relat. Mater. **18**, 1039 (2009).
[23]T. Q. Nguyen, H. A. Shih, M. Kudo, and T. Suzuki, Phys. Status Solidi C **10**, 1401 (2013).
[24]Y. Liu, J. Bardwell, S. McAlister, S. Rolfe, H. Tang, and J. Webb, Phys. Status Solidi C **0**, 69 (2003).
[25]H.-A. Shih, M. Kudo, M. Akabori, and T. Suzuki, Jpn. J. Appl. Phys. **51**, 02BF01 (2012).
[26]H.-A. Shih, M. Kudo, and T. Suzuki, Appl. Phys. Lett. **101**, eid043501 (2012).
[27]H.-A. Shih, M. Kudo, and T. Suzuki, J. Appl. Phys. **116**, eid184507 (2014).
[28]S. P. Le, T. Q. Nguyen, H. A. Shih, M. Kudo, and T. Suzuki, J. Appl. Phys. **116**, 054510 (2014).
[29]Y. L. Chiou and C. T. Lee, IEEE Trans. Electron Devices **58**, 3869 (2011).
[30]S. Ganguly, J. Verma, G. Li, T. Zimmermann, H. Xing, and D. Jena, Appl. Phys. Lett. **99**, 193504 (2011).
[31]M. Esposto, S. Krishnamoorthy, D. N. Nath, S. Bajaj, T.-H. Hung, and S. Rajan, Appl. Phys. Lett. **99**, 133503 (2011).
[32]M. Ťapajna and J. Kuzmík, Appl. Phys. Lett. **100**, 113509 (2012).
[33]J. Son, V. Chobpattana, B. M. McSkimming, and S. Stemmer, Appl. Phys. Lett. **101**, 102905 (2012).
[34]T. H. Hung, S. Krishnamoorthy, M. Esposto, D. N. Nath, P. S. Park, and S. Rajan, Appl. Phys. Lett. **102**, 072105 (2013).
[35]M. Ťapajna, M. Jurkovič, L. Válik, Š. Haščík, D. Gregušová, F. Brunner, E.-M. Cho, T. Hashizume, and J. Kuzmík, J. Appl. Phys. **116**, 104501 (2014).
[36]M. Matys, B. Adamowicz, A. Domanowska, A. Michalewicz, R. Stoklas, M. Akazawa, Z. Yatabe, and T. Hashizume, J. Appl. Phys. **120**, 225305 (2016).
[37]M. Ťapajna, L. Válik, F. Gucmann, D. Gregušová, K. Frohlich, Š. Haščík, E. Dobročka, L. Tóth, B. Pécz, and J. Kuzmík, J. Vac. Sci. Technol. B **35**, 01A107 (2017).
[38]G. Dutta, S. Turuvekere, N. Karumuri, N. DasGupta, and A. DasGupta, IEEE Electron Device Lett. **35**, 1085 (2014).
[39]Y. Li, Y. Guo, K. Zhang, X. Zou, J. Wang, Y. Kong, T. Chen, C. Jiang, G. Fang, C. Liu *et al.*, IEEE Trans. Electron Devices **64**, 3139 (2017).
[40]M. Akazawa and T. Hasezaki, Phys. Status Solidi B **255**, 1700382 (2018).
[41]J. Koba and J. Koike, AIP Adv. **12**, 085302 (2022).
[42]W. Choi, O. Seok, H. Ryu, H.-Y. Cha, and K.-S. Seo, IEEE Electron Device Lett. **35**, 175 (2013).
[43]T. E. Hsieh, E. Y. Chang, Y. Z. Song, Y. C. Lin, H. C. Wang, S. C. Liu, S. Salahuddin, and C. C. Hu, IEEE Electron Device Lett. **35**, 732 (2014).
[44]M. Hua, J. Wei, G. Tang, Z. Zhang, Q. Qian, X. Cai, N. Wang, and K. J. Chen, IEEE Electron Device Lett. **38**, 929 (2017).

[45]J. Garrido, J. Sanchez Rojas, A. Jimenez, E. Munoz, F. Omnes, and P. Gibart, Appl. Phys. Lett. **75**, 2407 (1999).
[46]O. Ambacher, B. Foutz, J. Smart, J. Shealy, N. Weimann, K. Chu, M. Murphy, A. Sierakowski, W. Schaff, L. Eastman *et al.*, J. Appl. Phys. **87**, 334 (2000).
[47]F. Bernardini, V. Fiorentini, and D. Vanderbilt, Phys. Rev. B **63**, 193201 (2001).
[48]E. Miller, E. Yu, C. Poblenz, C. Elsass, and J. Speck, Appl. Phys. Lett. **80**, 3551 (2002).
[49]A. Winzer, R. Goldhahn, G. Gobsch, A. Link, M. Eickhoff, U. Rossow, and A. Hangleiter, Appl. Phys. Lett. **86**, 181912 (2005).
[50]S. Mohney and X. Lin, J. Electron Mater. **25**, 811 (1996).
[51]K. Schweitz and S. Mohney, J. Electron. Mater. **30**, 175 (2001).
[52]E. H. Nicollian and J. R. Brews, *MOS (Metal Oxide Semiconductor) Physics and Technology* (John Wiley & Sons, 2002).
[53]Y. Hori, Z. Yatabe, and T. Hashizume, J. Appl. Phys. **114**, 244503 (2013).